Pharm Res (2014) 31:1194–1209
DOI 10.1007/s11095-013-1242-x

RESEARCH PAPER

Influence of Short-Chain Cell-Penetrating Peptides on Transport of Doxorubicin Encapsulating Receptor-Targeted Liposomes Across Brain Endothelial Barrier

Gitanjali Sharma • Amit Modgil • Tiecheng Zhong • Chengwen Sun • Jagdish Singh

Received: 28 August 2013 / Accepted: 20 October 2013 / Published online: 16 November 2013

ABSTRACT

Purpose To investigate the influence of different cell penetrating peptides (CPPs-TAT, Penetratin and Mastoparan), on the transport of doxorubicin encapsulating transferrin (Tf)-liposomes across brain endothelial barrier, *in vitro* and *in vivo*.

Methods The cellular uptake of dual-functionalized, (Tf-CPP), liposomes into various tumor cells was assessed using HPLC. The transport of liposomes was also measured across a robust 3D brain tumor model constructed using chitosan-PLGA scaffolds. The growth of tumor cells was monitored using H&E staining and the fully grown tumor scaffolds were visualized using SEM. The tumor scaffolds were combined with the culture inserts carrying tightly packed brain endothelial cells. The *in vitro* and *in vivo* transport of drug (using Tf-CPP-liposomes) across the brain endothelial barrier was determined by extraction of the drug from cells and tissues followed by analysis using HPLC.

Results The results demonstrated improved delivery of doxorubicin using dual-functionalized liposomes *versus* the single ligand or unmodified liposomes. Among different Tf-CPP-liposomes, the Tf-Penetratin liposomes showed efficient cellular transport of the encapsulated drug (approximately 90–98%) and maximum translocation of the drug across the brain endothelial barrier (approximately 15% across *in vitro* and 4% across *in vivo* BBB). The Tf-Penetratin and Tf-TAT liposomes demonstrated excellent cellular biocompatibility and no hemolytic activity upto 200nM phospholipid concentration.

Conclusions The Tf-CPP liposomes showed efficient translocation of the anticancer drug across the brain endothelial barrier. In addition, an absolute and robust *in vitro* brain tumor model was successfully constructed to overcome the practical intricacies of developing a successful *in vivo* orthotopic brain tumor model.

KEY WORDS blood brain barrier · cell penetrating peptides · dual-functionalized · liposomes · tumor

INTRODUCTION

The non-invasive transport of therapeutic molecules across the blood brain barrier (BBB) requires apposite harnessing of the canonical potential of nanotechnology in delivering therapeutic agents through formidable cellular barriers. The high impermeability and selectivity of the BBB prevent the transport of many therapeutic molecules into the brain and thus invalidate the influence of systemically administered drugs for the treatment of central nervous system (CNS) disorders (1,2). This has propelled exhaustive efforts in the area of developing expedient strategies for the delivery of therapeutics across the BBB. The conventional neurosurgery based methods including convection enhanced delivery (CED) and local injection or temporary disruption of BBB using hypertonic solutions are associated with the risk of infection and can cause neuropathological changes (3–5). Considering the limitations of invasive techniques for delivery

Electronic supplementary material The online version of this article (doi:10.1007/s11095-013-1242-x) contains supplementary material, which is available to authorized users.

G. Sharma · A. Modgil · T. Zhong · C. Sun · J. Singh
Department of Pharmaceutical Sciences
College of Pharmacy
Nursing and Allied Sciences
North Dakota State University
Fargo, North Dakota 58108, USA

J. Singh (✉)
Department of Pharmaceutical Sciences
College of Pharmacy, Nursing & Allied Sciences
North Dakota State University, Sudro Hall, Room 102A
Fargo, North Dakota 58108-6050, USA
e-mail: jagdish.singh@ndsu.edu

of therapeutics to brain, simple non-invasive strategies have become the focus of primary investigation.

Targeted delivery vectors can be administered systemically without causing physiological disruption of the BBB (6,7). Various receptors on the surface of BBB can be targeted for active delivery of small molecules, proteins or nucleic acids (8–10). The application of sterically stabilized Tf receptor targeted nanoparticles, for delivery to the brain, after parenteral administration has become well established over the past years (9–11). However, the delivery of molecules via sterically stabilized receptor targeted systems is limited by receptor saturation (12,13). In addition, the endocytic uptake of these nanoparticulate drug carriers eventually leads to lysosomal degradation (2,14). We previously demonstrated that conjugation of receptor targeted liposomes with long chain cell penetrating peptides (CPPs), like poly-L-arginine, resulted in improved cellular translocation, gene delivery and penetration across the BBB (12). However, the reduced cell viabilities, at higher liposomal concentrations, due to the greater cationic charge of long chain CPPs are anticipated to restrict their practical application. In the present study, we evaluated the effect of different short chain CPPs (HIV-1 TAT, Penetratin and Mastoparan) on the ability of Tf-liposomes to transport a water soluble drug, doxorubicin, into various tumor cells and across a novel and robust 3 dimensional (3D) *in vitro* brain tumor model. In addition, we analyzed the biodistribution of liposomes in adult Sprague Dawley (SD) rats.

CPPs are short amphipathic cationic peptides that facilitate rapid internalization of exogenous cargo like proteins, nucleic acids, liposomes, or nanoparticles. The concept of using CPPs for improving the delivery of molecules across the formidable cell membrane was established after finding enhanced transport of albumin into cells by using polylysine peptide (15). Later, the trans activator of transcription (TAT) from human immunodeficiency virus (HIV-1) was discovered followed by the emergence of various other CPPs of natural (AntP/Penetratin) and synthetic origin(Mastoparan/transportan) which were alternatively termed as protein transduction domains (PTDs) (16,17). Surface modification of liposomes with CPPs facilitates endosomal escape and increases their cellular delivery (15). The mechanism of internalization of these peptides is greatly dependent on the CPP used, the concentration, the type of cell line, and cargo carried. Although it is now known that the uptake of CPPs is mediated both via endocytic and non-endocytic pathways, the exact mechanism of cellular uptake still remains controversial. In this study, we have investigated the extent of cellular internalization and the mechanism of uptake of different CPP and Tf-CPP-liposomes in various cell types.

The complexities associated with the brain tumor pathology encumber the development of an *in vivo* brain tumor model. Prior efforts in designing the *in vitro* brain tumor models have been focused on the culture of tumor cells in three dimensional aggregates. Meng *et al.* (18) cultured the tumor cell aggregates on organotypic brain slices and evaluated the transport of fluorescent nanoparticles after directly adding the nanoparticles to the tumor tissue. Another group of scientists developed a 3D human brain tumor model by juxtaposing the glioma cell tumor spheriods with the non-tumor cell spheroids (19). However, the 3D cultures of tumor spheroids alone do not take into account the occurrence of brain endothelial barrier that limits the transport of therapeutic agents to brain. A recent report also indicated the role of brain endothelial barrier in regulating the transport of therapeutic agents for the treatment of brain tumor (20). In this study, we have employed a new approach to design an *in vitro* glioblastoma brain-tumor model where the transport of nanocarriers was gauged across the brain endothelial barrier into the 3D tumor cell cultures developed in porous scaffolds. The conditions were similar to the *in vivo* transport where the systemically administered delivery vector is required to overcome the BBB prior to reaching the target tumor tissue in the CNS.

Additionally, we evaluated the transport of different CPP conjugated Tf-liposomes (Tf-TAT, Tf-Penetratin and Tf-Mastoparan) across the *in vitro* brain tumor model. TAT and Penetratin have previously demonstrated efficient internalization of DNA, RNA, Proteins, nanoparticles etc. (21,22). Mastoparan is a 14-residue peptide from wasp (Vespula lewisii) venom and has been used in the construction of 21 residue peptide Transportan 10 (TP10) which has been widely investigated for the delivery of cargo, like proteins, into the cells (23). We combined the cell penetrating properties of these three CPPs with Tf-liposomes and investigated the ability of the Tf-CPP liposomes to deliver the desired drug, doxorubicin, in medulloblastoma (Daoy), glioblastoma (U87), and brain endothelial (bEnd.3) cells. The rationale for using these peptides was based on the difference in proportion of hydrophilic, amphiphilic, and hydrophobic amino acid residues in these three CPPs. TAT peptide consists of more hydrophilic amino acids, Penetratin has almost an equal proportion of hydrophilic and hydrophobic amino acids while Mastoparan consists of more hydrophobic amino acid residues. We performed a comprehensive investigation of the cellular uptake, mechanism of uptake, cytotoxic potential, and transport of the dual-functionalized, Tf-CPP liposomes across the *in vitro* brain tumor model. The anticancer drug doxorubicin was encapsulated in the liposomes for the evaluation of transport across *in vitro* and *in vivo* brain endothelial barrier. This drug was selected due to its hydrophicility, ease of analysis and inability to penetrate the BBB without the use of a lipophilic drug carrier (24).

MATERIALS AND METHODS

Materials

1,2-dioleoyl-3-trimethylammonium-propane chloride (DOTAP), 1,2-distearoyl-sn-glycero-3-phosphoethanolamine-N-[carboxy(PEG)2000](DSPE–PEG–COOH), and 1,2-Dioleoyl-sn-glycero-3-phosphoethanolamine (DOPE) were obtained from Avanti Polar Lipids (Birmingham, Alabama). HIV-1 TAT peptide, cholesterol, chitosan (50 kDa), amiloride hydrochloride, and 3-(4,5-dimethylthiazol-2-yl)-2,5-diphenyltetrazolium bromide (MTT) were procured from Sigma–Aldrich Company (St. Louis, Missouri). Penetratin and Mastoparan were obtained from Anaspec, Inc. (Fremont, California). Fetal bovine serum (FBS), phosphate buffered saline (PBS), and Dulbecco's modified Eagle medium (DMEM) were purchased from American Type Culture Collection (ATCC, Rockville, Maryland). Polyethylene terephthalate (PET) transwellculture inserts were procured from BD BioCoat™ (BD Biosciences, North Carolina). Poly (lactic-co-glycolide) (50:50; PLGA) was obtained from Polyscitech (West Lafayette, Indiana). N-Hydroxysuccinimide (NHS) and 1-ethyl-3-(3-dimethylaminopropyl) carbodiimide hydrochloride (EDC•HCl) were purchased from Alfa Aesar (Ward Hill, Massachusetts) and Creosalus Inc. (Louisville, Kentucky), respectively. Chlorpromazine HCl and colchicine were procured from Enzo Life Sciences (Farmingdale, New York). All other chemicals used in this study were of analytical reagent grade. Brain endothelial cell line, bEnd.3 was purchased from American Type Culture Collection (ATCC, Rockville, Maryland).

Preparation of Dual-Functionalized Liposomes

The dual-functionalized liposomes were prepared using post-insertion technique as previously reported (12). Briefly, the primary amine group of the CPPs was terminally conjugated to EDC/NHS activated DSPE-PEG$_{2000}$-COOH. The DSPE-PEG-CPP was then mixed with other phospholipids DOPE/DOTAP/cholesterol in chloroform: methanol (2:1) and dried to form a thin lipid film. The thin film was then hydrated using Hepes buffered saline, pH 7.4 to form CPP coupled liposomes (CPP-liposomes). Transferrin was coupled to the distal end of DSPE-PEG-COOH via EDC/NHS reaction to form Tf-micelles. The CPP-liposomes were then stirred overnight with Tf-micelles at room temperature to form Tf-CPP-liposomes. The free Tf-micelles were separated from the Tf-CPP liposomes by passing the liposomes through sepahadex G-100 column. The Tf-CPP-liposomes were characterized for size and charge using zetasizer. The coupling efficiency of transferrin to the liposomes was determined using microbicinchonic acid assay as described earlier (12). The conjugation of CPPs to the DSPE-PEG-lipid was confirmed using fluorescamine assay (25). Stock solution of fluorescamine (Fluram®) was prepared in acetone at a concentration of 1 mg/ml. A fixed volume (50 µl) of fluorescamine stock solution was added to each standard or sample prepared in sodium borate buffer, pH 8.5 (26,27). The standard curve was generated using varying concentrations of free CPPs. DSPE-PEG-lipid without CPP conjugation was used as a control. The fluorescence of the samples and standards was measured at excitation and emission wavelengths of 365 and 470 nm, respectively.

Doxorubicin Loading

Doxorubicin encapsulating liposomes were generated using pH gradient drug loading. As described above, the thin phospholipid film was hydrated using citric acid buffer, pH 5.0 (to form CPP-liposomes) followed by stirring with Tf-micelles in the citric acid buffer. The final liposomes were passed through sephadex G-100 column pre-equilibrated with Hepes buffered saline, pH 7.4 to remove any extra liposomal Tf-PEG-lipid and to exchange the extra liposomal citric acid buffer with the Hepes buffered saline. Therefore a pH gradient was generated between the outer aqueous buffer at pH 7.4 and the intra liposomal citric acid buffer at pH 5.0. The drug doxorubicin was added to the liposomal suspension and incubated at 50°C for 60 min. The drug loaded liposomes were then cooled to room temperature and passed through sephadex columns to remove the un-encapsulated drug. Encapsulation efficiency of the liposomes was determined using high performance liquid chromatography (HPLC). A solution of 10 µl of the liposomes, before and after passing through the column, was prepared in 380 µl of phosphate buffer (pH 5.5) with 10 µl of 0.1% triton X-100 and 100 µl of methanol. The samples were analyzed using HPLC system equipped with UV-visible detector (28). The analysis was performed at a wavelength of 234 nm using C18 column and phosphate buffer pH 5.5: Acetonitrile (75:25) mixture as mobile phase with a flow rate of 0.5 ml/min. In addition, doxorubicin release studies were performed by diluting the liposomal samples in PBS with 10% FBS and incubating the samples at 37°C (Supplementary Material Fig. S10). Samples were withdrawn at different time points, passed through sephadex columns and analyzed using HPLC.

Cytotoxicity Assay

The biocompatibility of the CPP-liposomes was evaluated in three different cell lines, Daoy (medulloblastoma), U87 (glioblastoma), and bEnd.3 (brain endothelial). The cytotoxic potential of the liposomes was assessed at 50, 100, 200, 400 and 600 nM concentrations of phospholipids. The details of the procedure were reported in our previous work (12). Briefly, all cell types were plated in 96 well plates at a density

of approximately 500 cells/well, 24 h prior to performing the MTT assay. Following this, the cells were exposed to different concentrations of either plain, Tf, CPP, or Tf-CPP liposomes in serum free media. After incubating the cells for 2 h with liposomes, the media containing liposomes was replaced with fresh serum containing media and the cells were incubated for a total time period of 48 h. The cells viability was evaluated by adding the MTT solution to the cells and incubating the cells for 3 h. Following this, the MTT solution was removed and the formazan crystals were dissolved in DMSO. The absorbance of the cells was measured at 570 nm. The control group consisted of untreated cells.

Cell Uptake

Cell uptake of doxorubicin loaded liposomes (Plain, Tf, CPP, and Tf-CPP-liposomes) was evaluated in the three cell lines: Daoy, U87, and bEnd.3 cells. Qualitative investigation of liposomal uptake was performed using fluorescence microscopy. The cells (6×10^4/well) were seeded onto 35 mm culture dishes 24 h prior to the uptake analysis. Doxorubicin encapsulating liposomes were incubated with the cells at a concentration of 100nM and the uptake of liposomes was investigated at different time intervals. Following liposomal uptake, the cells were rinsed with PBS, pH 7.4. The nuclei of the cells were stained with 4′,6-diamidino-2-phenylindole (DAPI) dye and fluorescence of the cells was evaluated using fluorescence microscope (Olympus, Melville, NY). The uptake of doxorubicin was quantified by lysis of the cells in triton X-100 followed by extraction in methanol. The solution was centrifuged at 3, 000 rpm for 15 min at 4°C and the supernatant was analyzed using HPLC system equipped with UV-visible detector. The analysis was performed as described above for evaluation of doxorubicin loading.

Uptake Mechanism

The mechanism of internalization of different liposomes was investigated using various membrane entry inhibitors. The cells (Daoy, U87, and bEnd.3) were cultured in 35 mm culture dishes and were incubated at 4°C to inhibit all energy dependent endocytic processes (29) or pretreated with either chlorpromazine (10 μ g/ml) to inhibit the formation of clathrin coated vesicles, colchicine (10 μM) to prevent the formation of caveolae (30), methyl-β-cyclodextrin (5 mM) to inhibit cholesterol dependent endocytic processes (31) or amiloride(50 μM) to inhibit macropinocytosis (32). After pretreatment of the cells with inhibitors for 30 min, the cells were incubated with the liposomes for about 1 h. The uptake of the doxorubicin encapsulating liposomes was evaluated microscopically and the uptake of drug was quantified using HPLC.

3-Dimensional (3D) Brain Tumor Model

The porous scaffold for the growth of tumor cells was generated using emulsion freeze drying technique (33). Poly(D,L-lactide-co-glycolide) (PLGA, lactic acid/glycolic acid 50:50) was dissolved in dichloromethane at a concentration of 0.2 g/ml. This solution (5 ml) was added to a mixture of 500 mg of Chitosan (50 kDa) and 150 mg poly vinyl alcohol (PVA) in 10 ml of acetic acid buffer, pH 4.5 at 2 ml/min with constant stirring using a glass rod. Five hundred microliter solution of collagen in 0.1 M acetic acid (0.1%w/v) was added to the above mixture with stirring to form an emulsified paste. The paste was then poured into rod shaped moulds and freeze dried to form the chitosan-PLGA scaffold. The scaffolds were sectioned into discs of 2 mm thickness which were used for the culture of tumor cells.

Growth of Tumor Cells in 3D Microenvironment

The scaffold discs were rinsed with PBS, pH 7.4 and the glioblastoma cells were added to the scaffold surface and incubated overnight. Fresh media containing 20–30% serum was added the following day and the cells were cultured for approximately 35 days to form 3D tumors on scaffold. The cellular biocompatibility was assessed using MTT assay and the cell growth was monitored by hematoxylin-eosin staining of the frozen scaffold sections. The scaffold sections, at different time points, were embedded in Tissue Tek OCT™ compound and snap frozen in dry ice. The scaffold with tumor cells was sectioned using cryostat, mounted on polylysine coated slides and stained using hemotoxylin-eosin (9). The scaffold was assessed for continuous pore formation and 3D tumor growth using scanning electron microscopy (SEM). The scaffold sections were attached to the sample stubs with carbon paint and were sputter coated with gold. These sections were evaluated under JEOL JSM-6490LV high-performance variable pressure SEM. The tumor cells growing in 3D environment on the scaffolds were then combined with the culture inserts (0.4 μm pore size) carrying bEnd.3 cells on the luminal surface of the insert membrane (12) to form a 3D brain tumor model. Culture inserts with brain endothelial cells were placed above the scaffold and different liposomes (TAT, Penetratin and Mastoparan peptides conjugated to Tf-liposomes) were evaluated for transport across the *in vitro* brain tumor model.

Evaluation of Liposomal Transport

The culture inserts seeded with mouse brain endothelial cells (bEnd.3) were placed above the tumor scaffolds on day 28 of tumor growth and cultured for about 7 days to form a brain-tumor barrier model. Brain tumor model was designed to simulate *in vivo* tumor conditions where the permeability of

the brain endothelial barrier is compromised by the glioblastoma tumor growth. The intactness of the barrier was determined by measuring the transendothelial electrical resistance (TEER) and the sodium fluorescein (Na-F) permeability coefficient across the endothelial cell layer. The TEER of culture inserts was measured using patch clamp technique (12,34). However, in this study the TEER values were determined across the endothelial cell layer on the culture inserts after removing the inserts from the scaffold containing wells and transferring them to the 24-well plates containing PBS (with Ca^{2+} and Mg^{2+} ions). The presence of scaffold with the inserts caused physical contact of the electrodes with the scaffold and interfered with the measurement of resistance resulting in very high resistance values. The Na-F permeability of the barrier was assessed by replacing the media inside the culture inserts with 500 µl of PBS, pH 7.4 containing 10 µg/ml of Na-F. The media in the lower compartment of the inserts, for the culture of tumor cells, was also replaced with PBS (pH 7.4). The paracellular transport of Na-F was assessed by measuring the fluorescence intensity of the samples from the upper and the lower compartment using fluorescence Spectra Max®M5 multimodal micro plate reader (Molecular devices, Sunnyvale, CA) at excitation/emission wavelength: 485/535 nm. Following transport, the scaffolds were rinsed with PBS and approximately 50 µl of 0.1% w/v Triton X-100 was added to tumor cells on scaffold with 500 µl of PBS, pH 7.4 and incubated for ~1 h at 37°C to lyse the tumor cells. The fluorescence of the lysate was measured at different time points to calculate the amount of Na-F transported across the endothelial barrier. The flux measured across cell free inserts and across the total model system was used to calculate the endothelial permeability coefficients (P_e) using the following equation (12,35,36):

$$1/P_e = 1/P_t - 1/P_f \text{cm/s} \quad (1)$$

where P_t and P_f are the apparent permeability coefficients across the total barrier system and cell free inserts, respectively. The permeability coefficients were assessed across the culture inserts with only endothelial cells and across the *in vitro* brain tumor model and were compared with the permeability coefficient values across the *in vitro* BBB model.

The liposomal transport was similarly assessed by adding different liposomes to the culture inserts seeded with brain endothelial cells and placed on the 3D tumor scaffolds. The media in surrounding the scaffold in the lower compartment was replaced with fresh serum containing PBS (pH 7.4). Also, the media inside the culture inserts was replaced with the liposomal suspensions (200nM) in 1 ml of fresh serum containing buffer. The doxorubicin containing liposomes were transported across the endothelial barrier into the 3D tumor cell mass growing within the porous scaffold. Following the transport of liposomes, the tumor cells were lysed as described above and the lysates were analyzed using HPLC system equipped with UV-visible detector. The analysis was performed at wavelength of 234 nm using C18 column and phosphate buffer pH 5.5: Acetonitrile (75:25) mixture as described earlier for cell uptake analysis.

Hemolysis Assay for Liposomes

The cationic lipids and cell penetrating peptides can potentially interact with the negatively charged membranes of the erythrocytes and cause hemolysis. The hemolysis assay was performed as previously reported (9). Briefly, the blood collected from an adult rat was centrifuged at 2,000 rpm for 10 min. The pelleted red blood cells were rinsed with PBS, pH 7.4 and the erythrocyte count was determined using hemocytometer. The liposomes were added to a pre-determined number of erythrocytes and incubated ay 37°C for 60 min. Following this, the samples were centrifuged at 2,000 rpm for 10 min and the absorbance of the supernatant was determined at 540 nm by spectrophotometric analyses. The absorbance of the supernatant from erythrocyte samples exposed to Triton X-100 and PBS were used as positive (100% hemolysis) and negative (0% hemolysis) controls, respectively. The percent hemolysis was calculated as:

$$\text{Hemolysis}(\%) = \left[\left(\text{Abs}_{(\text{exp})} - \text{A}_{(\text{PBS})}\right)/\text{Abs}_{(\text{T})}\right] * 100 \quad (2)$$

where $\text{Abs}_{(\text{exp})}$, $\text{Abs}_{(\text{PBS})}$ and $\text{Abs}_{(\text{T})}$ are the absorbance of the experimental samples, PBS and Triton X-100, respectively. Less than 10% hemolysis was considered non-toxic. All experiments were performed in quadruplicate to obtain statistically relevant results.

In Vivo Biodistribution of Liposomes

All animal experiments were carried out in accordance with the guidelines outlined by the Institutional Animal Care and Use Committee (IACUC) at North Dakota State University (Protocol #A12024). Biodistribution of the liposomes was evaluated in adult Sprague–Dawley rats. The animals were kept under controlled temperature conditions with 12 h light and dark cycles and were allowed free access to food and water. After 7 days of acclimation period, the rats were intravenously injected with either free doxorubicin or doxorubicin loaded liposomes. Animals were divided into 7 groups and each group was injected with either free doxorubicin, doxorubicin loaded plain, Tf, Tf-TAT, Tf-Penetratin, or Tf-Mastoparan liposomes at a dose of 15.2 µmoles of phospholipids/kg body weight. Animals injected with PBS, pH 7.4 were used as control. At time points of 12, 24 and 48 h various organs including brain, liver, heart, lungs, kidneys and spleen were isolated and blood samples were withdrawn. The distribution of drug to various

organs was determined by homogenization of tissue samples and extraction of the drug in chloroform: methanol (3:1). The extracted samples were then dried in a vacuum drier and the residue was reconstituted in phosphate buffer pH 5.5: methanol (4:1). The reconstituted samples were vortexed to allow complete re-suspension of the residue followed by centrifugation of the samples at 10,000 rpm and 4°C to remove any unwanted proteins. The supernatant was then analyzed using HPLC system equipped with UV-visible detector at 234 nm as described for cell uptake analysis. A standard curve for the measurement of the drug extracted from each organ was generated by vortexing free doxorubicin in methanol with the tissue samples from different organs of control rat. The samples were homogenized and the drug was extracted as illustrated above. All data were normalized in units of percentage of injected dose per gram of the tissue (%ID/g).

Statistical Analysis

The statistical data were processed using Microsoft Excel 2010 software and presented as mean ± standard deviation (S.D.)($n=6$). The treatment and control groups were compared using two tailed student's t-test and analysis of variance.

RESULTS

Characterization of Liposomes

The overall size of all the liposomes was less than 200 nm and the zeta potential of the dual-functionalized liposomes was in the near neutral range. Table I summarizes the size and overall charge of different liposomes. The results showed that conjugation of transferrin protein to the liposomes significantly ($p<0.05$) increased the particle size of the liposomes. The sizes of TAT, Penetratin, and Mastoparan conjugated liposomes did not differ significantly ($p>0.05$) from each other. The overall charge of the CPP conjugated liposomes was positive, however, the conjugation of transferrin protein to the CPP-liposomes neutralized the cationic charge of the CPPs thus, imparting near neutral characteristics to the liposomes. The zeta potential of the transferrin liposomes was negative which could be attributed to the presence of negatively charged protein on the surface of the liposomes. No significant ($p>0.05$) change in size of Tf-CPP liposomes was observed after incubation of the liposomes at 37°C in PBS containing 10% serum. However, the size of CPP-liposomes increased significantly ($p<0.05$) after incubation in PBS containing serum (Supplementary Material Table S1). This was ascribed to the adsorption of negatively charged serum proteins onto CPP-liposomes (due to the presence of only cationic CPPs on the liposomal surface leading to higher positive zeta potential). The presence of polyethylene glycol on the liposomes prevented their aggregation in the presence of serum. However, the presence of serum proteins in the buffer resulted in slightly negative zeta potential values.

Table I Particle Size and Zeta Potential of the Liposomes

Liposomes	Particle size (nm)	Zeta potential (mV)	PDI[a]
Plain	172.3 ± 3.768	6.58 ± 3.27	0.258 ± 0.014
TAT	176.7 ± 4.7055	19.07 ± 2.82	0.242 ± 0.008
Tf	185.6 ± 8.403	−8.151 ± 4.961	0.404 ± 0.037
Tf-TAT	183.0 ± 6.418	13.16 ± 3.801	0.319 ± 0.038
Tf-Mast	188.3 ± 8.214	11.28 ± 5.729	0.212 ± 0.042
Mast	175.2 ± 3.212	16.826 ± 2.816	0.231 ± 0212
Pen	178.7 ± 7.713	21.202 ± 2.471	0.218 ± 0.065
Tf-Pen	186.82 ± 9.214	15.28 ± 5.312	0.201 ± 0.073

Data are presented as mean ± SD from at least four different preparations

[a] *PDI* poly dispersity index

Micro BCA assay revealed a Tf content of approximately 69.82 ± 5.2%, 63.21 ± 5.1%, 60.13 ± 4.9%, and 61 ± 5.8% for Tf-liposomes, Tf-TAT, Tf-Mastoparan and Tf-Penetratin liposomes, respectively. Fluorescamine assay showed a coupling efficiency of approximately 85 ± 4.3%, 82.88 ± 5.2% and 83.31 ± 4.8% for TAT, Penetratin and Mastoparan, respectively. The drug encapsulation efficiencies were observed to be 78 ± 5.3%, 74.82 ± 4.6%, 76.33 ± 3.8%, and 77.98 ± 4.3% for plain, TAT, Penetratin, and Mastoparan liposomes, respectively. The doxorubicin encapsulation efficiencies were 68.38 ± 6.3%, 65.81 ± 5.2%, and 66.73 ± 5.8% for Tf-TAT, Tf-Penetratin and Tf-Mastoparan liposomes, respectively.

Biocompatibility of Liposomes

The liposomes, without doxorubicin, were observed to be non-toxic in all three cell lines and showed a cell viability of approximately 80–90% upto a phospholipid concentration of 200nM (Supplementary Material Fig. S1). The cell viabilities were observed to be lower with Tf-Mastoparan liposomes at higher concentrations in all three cell lines. The viabilities at 600 nM concentration were observed to be approximately 71.6%, 59.8% and 56.8% in Daoy, U87 and bEnd.3 cells, respectively. Furthermore, the viabilities were higher in the tumor cell lines (Daoy and U87) as compared to the brain endothelial (bEnd.3) cells. Also, U87 cells were found to be more sensitive to liposomal exposure as compared to the Daoy cells. In contrast, the negatively charged Tf-liposomes showed higher cell viabilities (approximately 90.23–95.48%), irrespective of the type of cells. The cell viabilities were observed to decrease significantly ($p<0.05$) after

encapsulation of doxorubicin (Fig. 1). The cytotoxicity of Tf–TAT liposomes was least while Tf-Mastoparan liposomes showed maximum cytotoxic potential. In addition, a significant ($p < 0.05$) decrease in cell viability was observed at higher concentrations with all liposomes. Tf-Mastoparan liposomes showed a cell viability of approximately 13–18% at 600nM concentration in all three cell lines. The cell viability of Tf-TAT liposomes decreased from approximately 75.7–35.6% with an increase in phospholipid concentration from 50nM to 600nM concentration in Daoy cells. The cell viabilities of the single ligand CPP-liposomes were lower as compared to the dual-functionalized, Tf-CPP or plain liposomes (Supplementary Material Fig. S2)

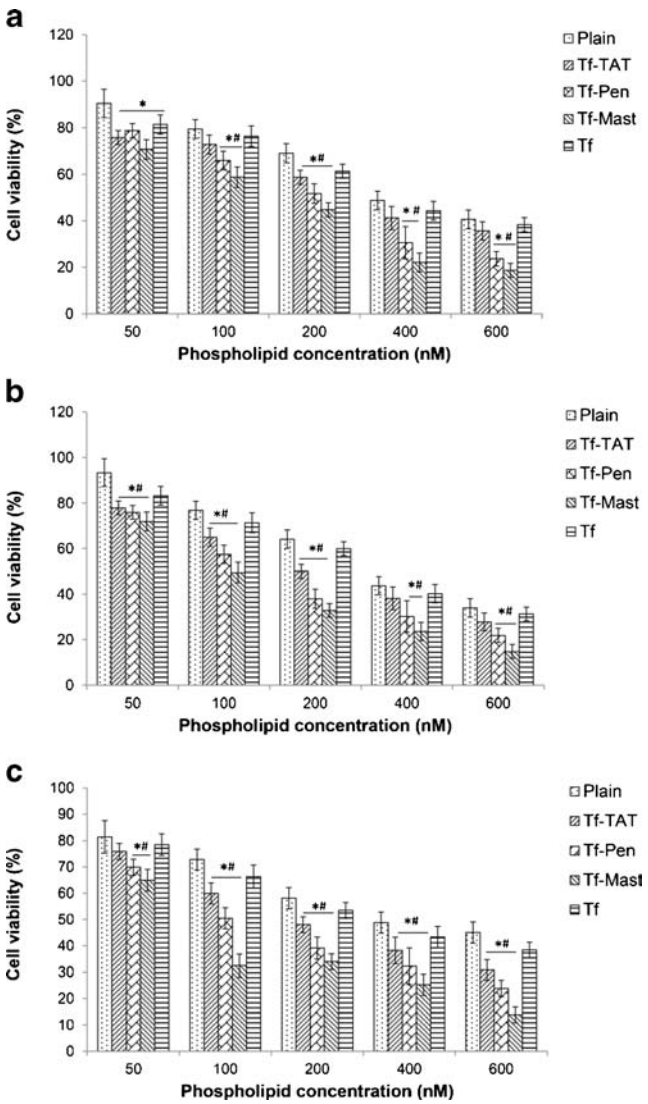

Fig. 1 Bar graph depiction of the viabilities of (**a**) Daoy, (**b**) U87 and (**c**) bEnd3 cells after exposure to doxorubicin encapsulating plain and dual-functionalized liposomes. The cells exposed to different liposomes were evaluated for cytotoxicity using MTT assay. The data are presented as mean ± S.D. ($n = 4$); Statistically significant ($p < 0.05$) differences are indicated in comparison with (*asterisk*) plain and (*number sign*) Tf-liposomes at the respective concentrations.

Cell Uptake Analysis

We exploited the presence of transferrin receptors on the three cell lines (Daoy, U87 and bEnd.3) for delivery of Tf-CPP liposomes. Figure 2 illustrates the transport of different liposomes in the three cell lines following 1 h of incubation. Free drug demonstrated negligible uptake after incubation with the cells (Supplementary Material Fig S3 and S4). Plain liposomes, in the absence of any surface modification, showed the lowest transport in all types of cells while the dual-functionalized Tf-CPP liposomes showed maximum uptake and therefore, the strongest fluorescence pattern in all cells (Fig. 2a). Also, the uptake of Tf-liposomes was more than plain and CPP-liposomes. The uptake of liposomes was observed to increase with time (Supplementary Material Fig. S5).

Quantitative estimation of liposomal uptake further confirmed the efficacy of dual-functionalized liposomes over single ligand and plain liposomes (Fig. 2b). Tf-TAT liposomes showed an uptake of about 90%, 82% and 77% in U87, Daoy, and bEnd.3 cells, respectively. The uptake of Tf-Penetratin liposomes was about 98%, 96%, and 89% while the uptake of Tf-Mastoparan liposomes was about 97%, 90% and 87% in U87, Daoy, and bEnd.3 cells, respectively. The order of increasing fluorescence intensity for dual-functionalized liposomes was Tf-TAT < Tf-Mastoparan < Tf-Penetratin. In addition, the dual-functionalized liposomes also showed efficient gene expression in Daoy, U87, and bEnd.3 cells after transfection with liposomes encapsulating either green fluorescent protein or β-galactosidase expressing plasmid (Supplementary Material Fig. S6 and S7). The results emphasized the significance of dual-mechanism of uptake over receptor targeting or cell penetration alone.

Mechanism of Uptake

The uptake of all types of liposomes was almost completely inhibited at 4°C thus indicating an energy dependent uptake of the liposomes in all three cell lines (Fig. 3). Colchicine, an inhibitor of caveolae formation, did not inhibit the uptake of plain, Tf, or Tf-CPP liposomes. Also, macropincytosis inhibitor amiloride did not significantly ($p > 0.5$) inhibit the uptake of Tf-TAT, Tf-Penetratin, Tf, or plain liposomes. However, a significant ($p < 0.05$) reduction in the uptake of Tf-Mastoparan liposomes was observed using amiloride, thereby indicating the contribution of Mastoparan in the macropinocytic uptake of the liposomes into all three cell lines. Some inhibition (non-significant) of other Tf-CPP liposomes was also observed in the presence of amiloride. However, plain and Tf-liposomes were not affected by the macropinocytic inhibitor thus eliminating macropinocytosis as the uptake pathway for these liposomes. In contrast, the uptake of single ligand CPP-liposomes was considerably affected by the presence of amiloride and chlorpromazine

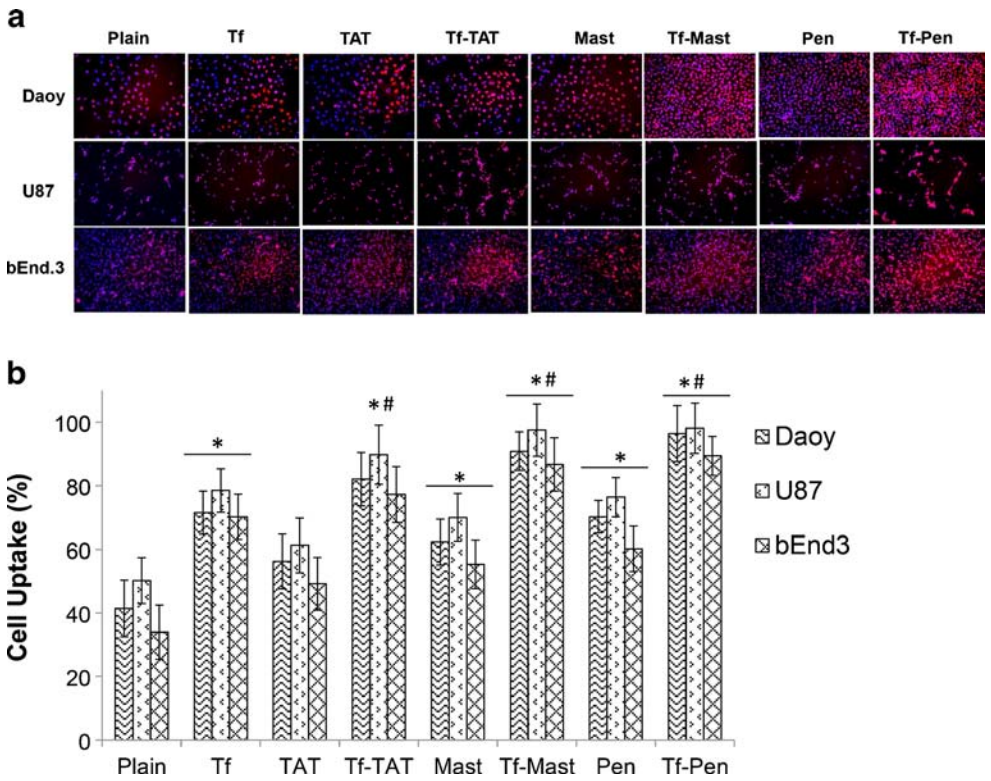

Fig. 2 (**a**) Fluorescence microscopic images (10× magnification) of different cells after uptake of doxorubicin encapsulating liposomes (excitation/emission wavelengths: 470/585 nm). The nuclei of the cells were stained with DAPI (excitation/emission: 330–385/420 nm). The image shows an overlap of the cells after uptake of doxorubicin liposomes (*red*) and the nuclei of the cells (*blue*); (**b**) bar graph representation of the uptake of doxorubicin liposomes after 1 h of incubation with either Daoy, U87, or bEnd3 cells. Following uptake, the cells were lysed and the uptake of liposomes was determined using high performance liquid chromatography (HPLC) equipped with UV visible detector at 234 nm. The results are expressed as mean ± S.D (n = 5). Statistically significant ($p < 0.05$) differences are indicated *versus* plain liposomes (*asterisk*) and Tf liposomes (*number sign*).

(Supplementary Material Fig. S8). In addition, chlorpromazine reduced the uptake of all types of liposomes to approximately 30–50% in all cell lines thereby illustrating clathrin-mediated uptake as the major pathway for uptake of liposomes. M-β-CD (methyl-β-cyclodextrin) depletes cholesterol, which is involved in the formation of invaginations leading to the development of clathrin-coated vesicles during the uptake of extracellular components (37). A significant ($p < 0.05$) reduction in the uptake of liposomes was observed using m-β-CD, thus re-confirming the participation of clathrin-coated vesicles in the uptake of liposomes. The results indicated clathrin-mediated uptake as the major pathway for the transport of plain, Tf and Tf-CPP liposomes. The uptake of free drug was only slightly inhibited at 4°C, thus indicating a non-energy dependent uptake as the major pathway for transport of free doxorubicin.

Design of 3D Brain Tumor Model

The scanning electron microscopic (SEM) images confirmed the formation of a porous scaffold and the growth of tumor spheroids inside the pores after approximately 35 days of culture in high serum containing media (Fig. 4). The scaffold showed excellent cellular biocompatibility and a considerable improvement in cell growth with time as observed with hematoxylin-eosin staining. Dense growth of overlapping tumor cells was observed on 20 μm thick sections of the scaffold on day 35 (Fig. 5). The 3D tumor culture was combined with the inserts (0.4 μm pore size) carrying brain endothelial cells cultured on the luminal side of the membrane. In our previous report, we demonstrated a significantly lower ($p < 0.05$) paracellular transport of Na-F across the *in vitro* BBB model constructed using both bEnd.3 cells and primary glial cells as compared to the model without glial cells (12). In this study, we observed a significant reduction in the paracellular transport of Na-F across the bEnd.3 cells on culture inserts combined with glioblastoma tumor scaffolds ($P_e = 3.96 \times 10^{-6}$) as compared to the transport of the fluorescent molecule across the inserts with bEnd.3 cells alone ($P_e = 7.93 \times 10^{-6}$) (Supplementary Material Fig. S9). However, the paracellular transport across the *in vitro* 3D tumor model was greater than the *in vitro* BBB model with primary glial cells on the underside of the membrane ($P_e = 1.98 \times 10^{-6}$). In addition, the TEER value of the endothelial cell layer cultured with the 3D tumor (226 ± 14 Ωcm^2) was higher than the TEER across the endothelial cell layer

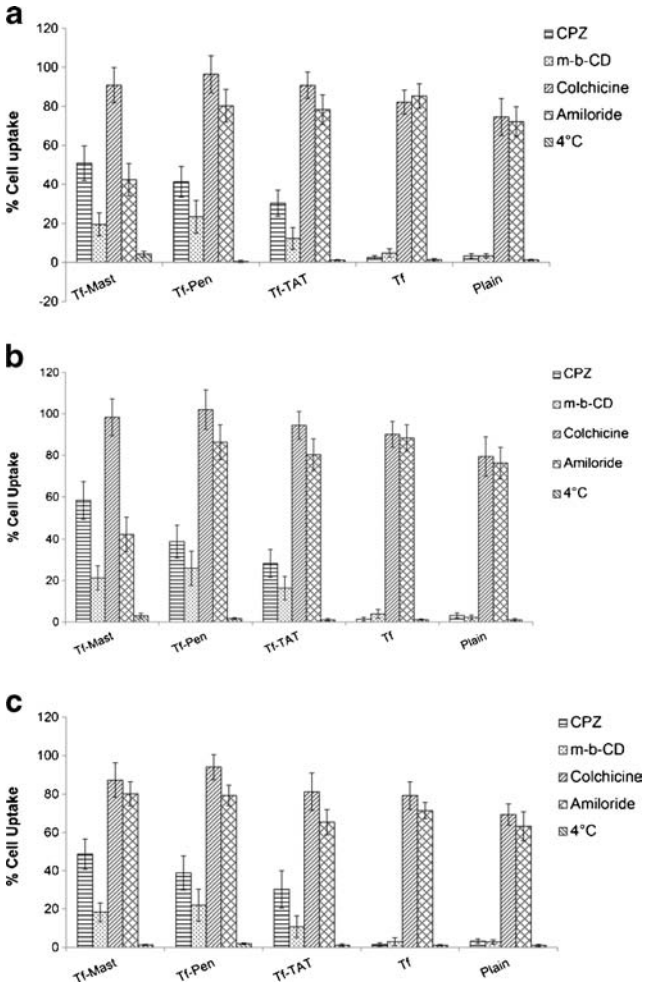

Fig. 3 Graphical representation of effect of various inhibitors on the uptake of doxorubicin encapsulating CPP-liposomes in (**a**) Daoy, (**b**) U87, and (**c**) bEnd3. The uptake of doxorubicin liposomes was quantified by lysis of the cells and measurement of the drug using HPLC system equipped with UV visible detector at 234 nm. The results are expressed as mean ± S.D. ($n = 4$).

cultured alone ($192 \pm 23\ \Omega cm^2$) but was lower than the TEER across the *in vitro* BBB model with endothelial cells on the upper side and the glial cells on the underside of the membrane ($323 \pm 16\ \Omega cm^2$).

Transport of Liposomes Across 3D Brain Tumor Model

The transport of dual-functionalized Tf-CPP liposomes was observed to be significantly ($p < 0.05$) higher in comparison to the single ligand Tf or CPP liposomes. The transport of plain liposomes was the lowest and was comparable to that of the free drug. Tf-Penetratin liposomes showed the highest endothelial permeability coefficient ($P_e = 5.52 \times 10^{-6}$) which was not significantly different ($p > 0.05$) from the Tf-Mastoparan liposomes ($P_e = 4.89 \times 10^{-6}$) (Fig. 6a). The percentage of liposomes transported increased from approximately 4.2% for TAT to 10.6% for Tf-TAT liposomes, from 5.4% for Mastoparan to 13.9% of Tf-Mastoparan liposomes, and from 6.5% for Penetratin to 14.9% for Tf-Penetratin liposomes (Fig. 6b). Therefore, dual modification considerably improved the transport across the *in vitro* brain tumor model. Additionally, the scaffolds were embedded into Tissue Tek OCT™ compound (Sakura Finetek USA, Inc., Torrance, CA) and sectioned on a cryostat to evaluate the uptake of doxorubicin liposomes by tumor cells growing in a 3D microenvironment (Fig. 7). Maximum fluorescence was observed in tumor scaffolds exposed to Tf-Penetratin liposomes. The results further justified the incorporation of CPP to Tf liposomes and triggering of the dual mechanism of transport via both receptor-mediated transcytosis and improved cell penetration.

Hemolysis Assay

Since the liposomes were designed to be injected intravenously into adult SD rats, we evaluated their interaction with the erythrocytes *in vitro* prior to the *in vivo* biodistribution analysis. The release of hemoglobin increased with increasing concentration of phospholipids (Fig. 8). Less than 10% hemolysis was considered non-toxic (9). Plain, Tf-Penetratin, and Tf-TAT liposomes were observed to be non-toxic upto a concentration of 600 nmol of phospholipids/ 1.5×10^7 erythrocytes. Slight hemolysis was observed with

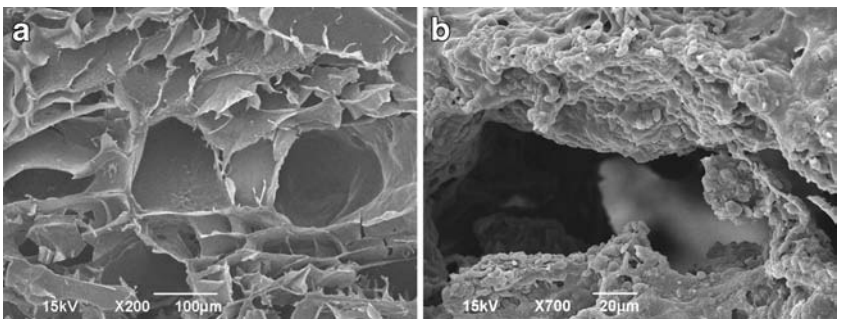

Fig. 4 SEM images showing (**a**) porous structure chitosan-PLGA scaffold and (**b**) tumor cells growing in a 3 dimensional environment within the pores of the scaffold. Cross sections of the scaffolds were cut diagonally across the edge of the sample. The sections were then mounted on aluminum mounts with colloidal silver paste and coated with a conductive layer of gold-palladium using Balzers SCD 030 sputter coater (BAL-TEC RMC, Tucson AZ). Images were obtained using a JEOL JSM-6490LV scanning electron microscope (JEOL USA, Peabody MA) at an accelerating voltage of 15 keV.

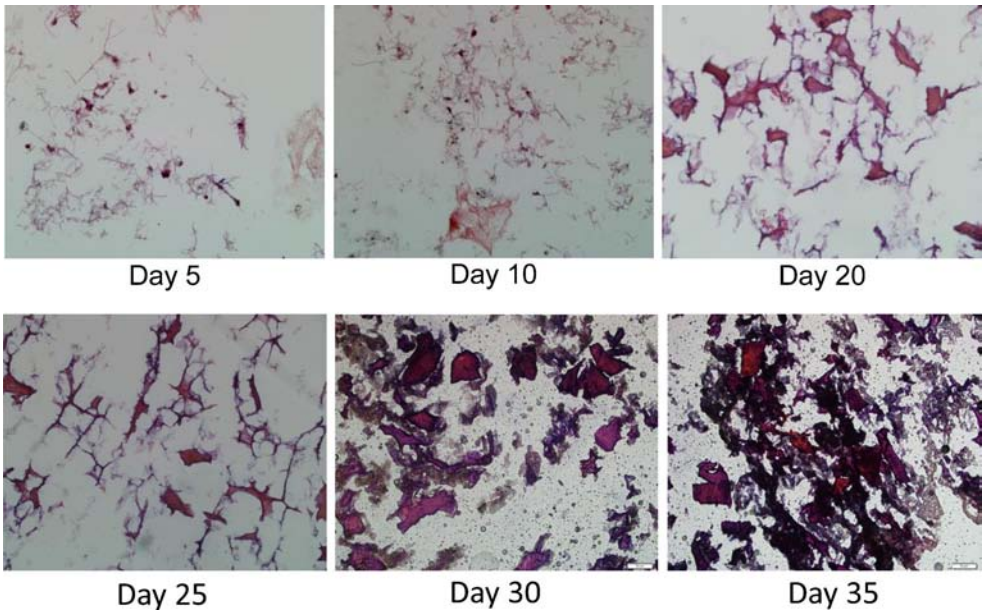

Fig. 5 Histological evaluation of tumor cell proliferation on porous scaffolds at different time points. The image shows hematoxylin-eosin staining of 20 μm thick sections of scaffolds with tumor cells growing in 3 dimensional environment in the porous scaffold. The images were captured at 10× magnification using light microscope equipped with 12.8 megapixel digital color camera.

Tf-Penetratin liposomes at concentration of 800 nmol of phospholipids. However, Tf-Mastoparan liposomes showed a significantly higher ($p < 0.05$) cytotoxicity at a concentration of 200 nmoles of phospholipids.

In Vivo Biodistribution

Considering the poor transport of CPP-liposomes across the *in vitro* brain tumor model, these liposomes were not evaluated for *in vivo* transport to brain. Doxorubicin loaded plain liposomes were used as a passive control. HPLC analysis of tissue samples indicated maximum accumulation of Tf conjugated liposomes in the spleen and liver 12 h post intravenous administration (Fig. 9). The %ID (percent injected dose) of the liposomes per gram of tissue decreased with increasing time intervals in all organs. Free doxorubicin and plain liposomes were eliminated more rapidly from the liver and spleen as compared to the Tf-CPP liposomes. Tf-

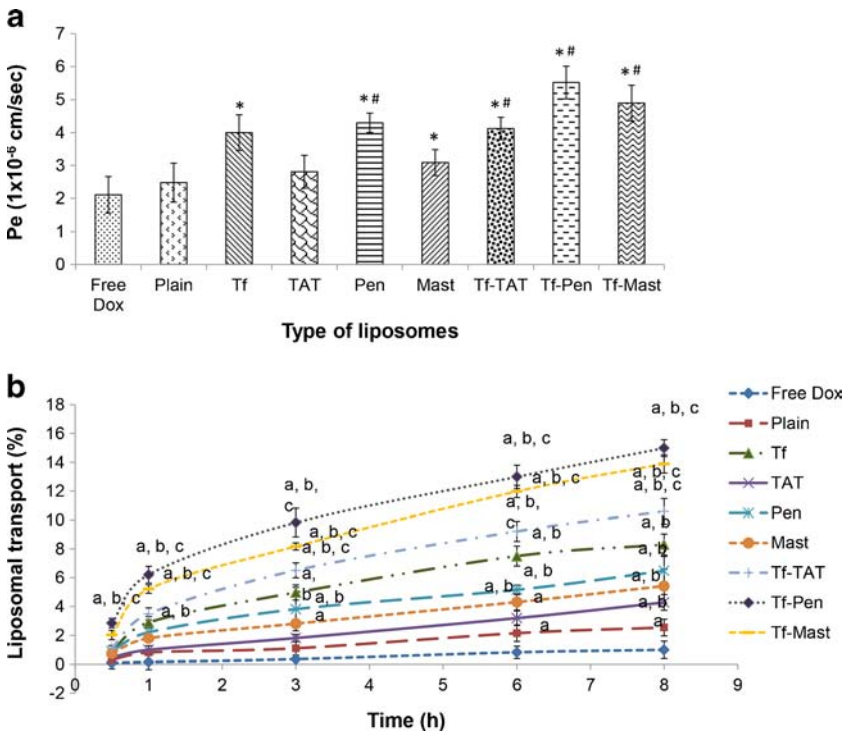

Fig. 6 (**a**) Endothelial cell permeability (Pe, expressed in $1 \times 10-6$ cm/s) coefficient for different liposomal formulations. All data are presented as mean ± S.D. ($n = 5$). Statistically significant differences ($p < 0.05$) are indicated in comparison with free doxorubicin (*asterisk*) and plain liposomes (*number sign*); (**b**) graphical representation of the percent transport of different doxorubicin encapsulating liposomes across in-vitro brain tumor model, over a period of 8 h. The tumor cells were lysed and analyzed using HPLC for transport of liposomes across the endothelial barrier. All data are presented as mean ± S.D. ($n = 5$). Significantly ($p < 0.05$) greater transport are indicated in comparison to free drug (*a*), plain (*b*), Tf (*c*).

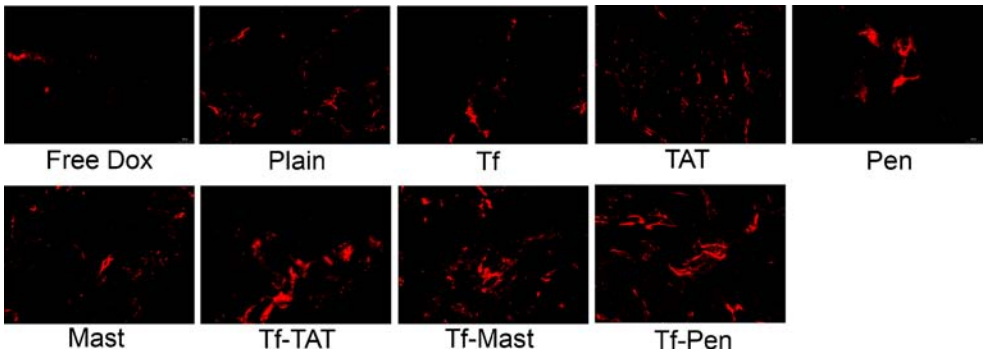

Fig. 7 Microscopic images (10× magnification) of tumor cells growing on scaffold sections after transport of various doxorubicin encapsulating liposomes. The images show 20 μm thick sections of the scaffolds with tumor cells after 8 h of liposomal transport.

Mastoparan liposomes showed a higher elimination from the major macrophage organs including the liver and spleen as compared to Tf-TAT or Tf-Penetratin liposomes. Tf-Penetratin liposomes were transported more to the heart and their elimination from heart was slower as compared to the other liposomes. The transport of Tf-Mastoparan liposomes to the lungs was slightly higher as compared to the Tf-Penetratin liposomes, nevertheless, the elimination of Tf-Mastoparan liposomes was more rapid than the Tf-Penetratin liposomes. Previous studies reported greater interaction of cationic polymers and CPPs with the blood cells and their subsequent accumulation in lungs (9,38). In this study, approximately 10–15% of the dual-functionalized liposomes were transported to the lungs after 24 h. The elimination of negatively charged Tf-liposomes was slower from liver, spleen and kidneys as compared to plain or dual-functionalized liposomes. The dual-functionalized, Tf-Penetratin liposomes showed maximum brain penetration after 24 h (~3.67% ID/gram of tissue) followed by the Tf-TAT liposomes (~2.89% ID/gram of tissue). The accumulation of Tf-Mastoparan liposomes was lower as compared to the other Tf-CPP liposomes in brain.

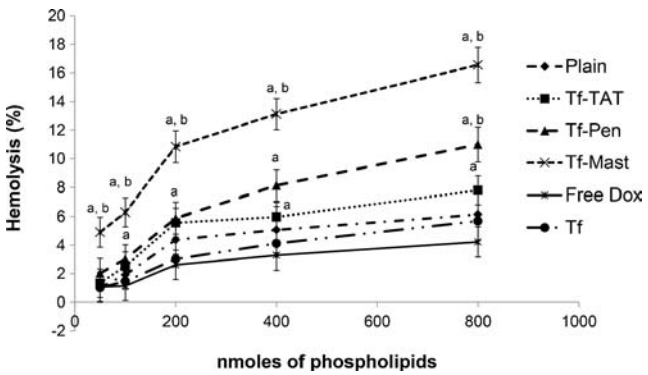

Fig. 8 Graph showing the hemolytic activity (%) of various liposomal formulations. Red blood cells were exposed to PBS and triton X-100 for negative and positive controls, respectively. Less than 10% hemolysis was considered non-toxic. Statistically significantly ($p < 0.05$) differences are reported in comparison to free drug (**a**) and plain liposomes (**b**). Data are presented as mean ± S.D. ($n = 5$).

DISCUSSION

The efficacy of a delivery device, for the treatment of brain tumor, is assessed based on its ability to penetrate the brain endothelial barrier and translocate to the tumor tissue. While considerable efforts have gone into the development of successful vectors for delivery across BBB, the transport of water soluble therapeutics into brain still remains a challenge. Although, the application of targeted delivery vehicles for site specific transport of molecules has long been embraced, the concept of improving the delivery of targeted vehicles using CPPs is nascent and the long term success of using CPPs depends on their detailed investigation under *in vitro* and *in vivo* conditions. In our previous report, we used poly-L-arginine (PR) as the CPP and demonstrated about 8 fold higher penetration of the dual-modified, Tf-PR-liposomes in rat brain as compared to the plain liposomes and about 2 fold higher transport in comparison to the single ligand, Tf-liposomes (9). However, the hemolytic activity and *in vitro* cytotoxicity of poly-L-arginine presented a limiting factor to the plausible application of higher concentrations of these liposomes. The Tf-PR liposomes showed a viability of approximately 70–78% in glial and brain endothelial cell lines, at 200nM phospholipid concentration (12). In comparison, the Tf liposomes conjugated to low molecular weight CPPs demonstrated cell viabilities of approximately 80–86%, at the same concentration. Also, the Tf-PR liposomes showed no hemolytic activity (less than 10% hemolysis) up to 600nM phospholipid concentration whereas, the Tf-TAT and Tf-Penetratin liposomes demonstrated hemocompatibility upto 800nM phospholipid concentration. As described above, the Tf-matsoparan liposomes showed greater toxicity, both *in vitro* and *in vivo*. The most likely cause of the low biocompatibility of the Tf-PR-liposomes was the presence of large number of cationic arginine residues in the high molecular weight long chain peptide, poly-L-arginine (39). In this study we have performed a detailed analysis of the influence of short chain cationic CPPs: TAT, Penetratin and Mastoparan, on the cellular penetration and biocompatibility of Tf-receptor targeted liposomes.

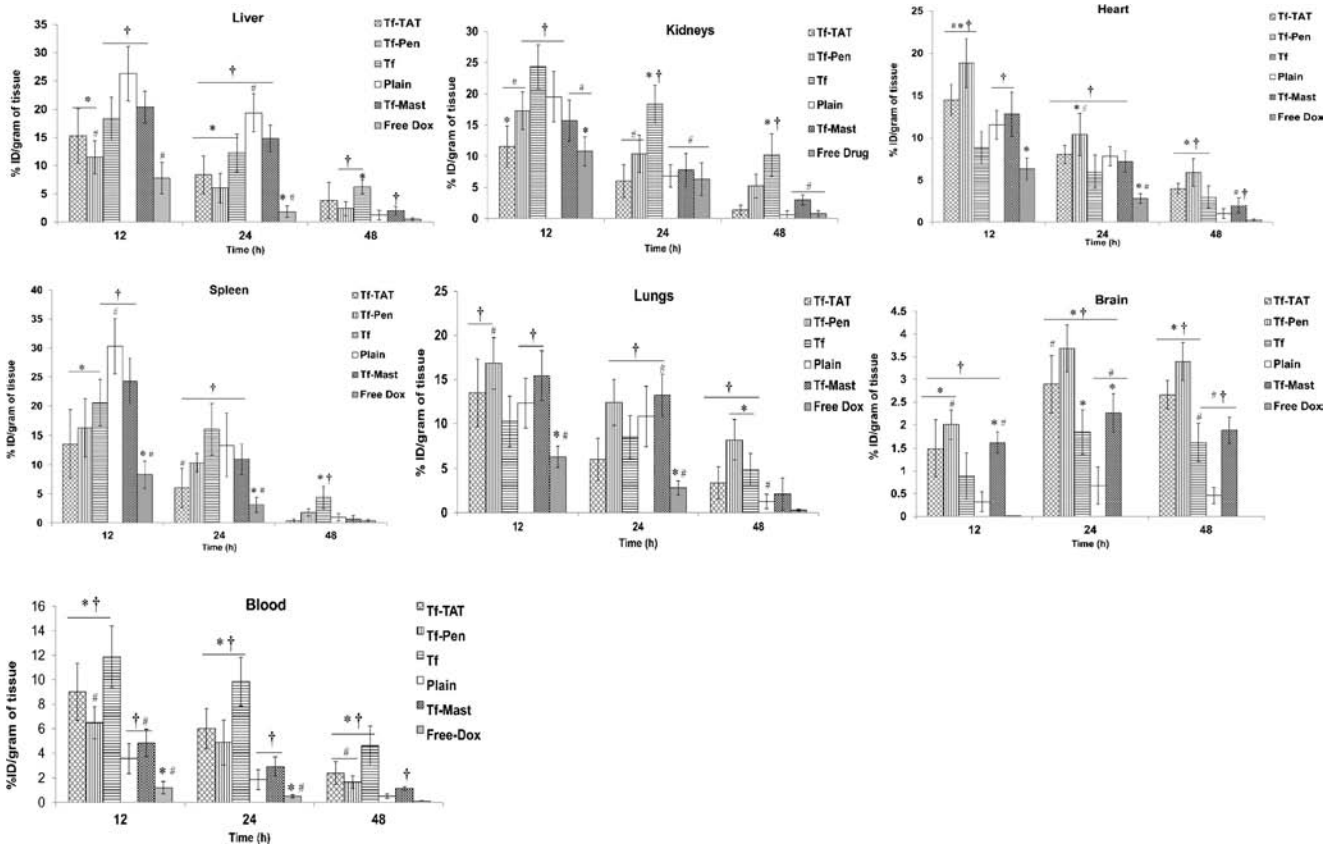

Fig. 9 Bar graphs showing the biodistribution of doxorubicin containing liposomes at various time points. The results are expressed as % injected dose (ID)/gram body weight (mean ± SD), $n = 6$. Statistically significant ($p < 0.05$) differences are indicated in comparison with (*dagger*) free doxorubicin, (*asterisk*) plain and (*number sign*) Tf-liposomes and at the respective concentrations. The rats were intravenously injected with liposomes at a dose of 5 mg of doxorubicin/kg body weight.

Surprisingly, despite the dubiousness associated with the feasibility of developing an *in vivo* brain tumor model, very little or no research has been done to develop efficient *in vitro* brain tumor models where the transport to the tumor is regulated via the endothelial barrier. In this study, we designed an *in vitro* brain tumor model using biodegradable chitosan-PLGA scaffolds where the transport of liposomes to the 3-dimensional tumor was regulated via the endothelial cells cultured on transwell inserts. Figure 10 illustrates the diagrammatic representation of the transport of Tf-CPP liposomes across 3D brain tumor model. The transport of dual-functionalized liposomes was assessed in the presence of 10% serum in order to mimic the *in vivo* conditions of high serum content.

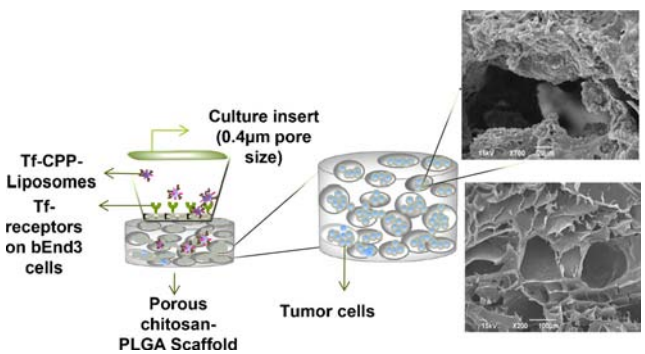

Fig. 10 Pictorial representation of the transport of dual-functionalized (Tf-CPP) liposomes across, the endothelial cell barrier, into the tumor cells growing in the porous structure of scaffold.

The simple and flexible method of synthesizing the dual-functionalized liposomes using post-insertion technique has been reported to result in efficient insertion of biologically active ligands into preformed liposomes (40). This method overcomes the limitations of the conventional process of conjugating the ligands with liposomes which is associated with a high probability of leaving unreacted functional groups and coupling reagents within the liposomes, thereby causing degradation of the encapsulated agent (40,41). The nano sized liposomes prepared using post-insertion technique possessed near neutral zeta potential (0–15 mV) and were therefore, anticipated to show lower elimination by the macrophage system (42,43). No significant ($p > 0.05$) difference in the encapsulation efficiencies of dual-functionalized liposomes was observed, however, the loading of plain and CPP modified liposomes was slightly higher (non-significantly) than the dual-functionalized liposomes. This might be due to the interference in the transport of drug molecules into preformed liposomes, via pH gradient loading, due to the presence of transferrin protein on the surface. In addition, the Tf-CPP

liposomes showed less than 31% of the drug leakage after 12 h of incubation in PBS (pH 7.4) in the presence of serum, at 37°C (Supplementary Material Fig S10) . The percent cumulative release of the drug was greater with plain liposomes as compared to the Tf and Tf-CPP liposomes. This was due to the presence of negatively charged protein, transferrin, which reduced the interaction of the Tf and Tf-CPP liposomes with serum proteins. Also, the higher positive charge of Penetratin contributed to greater interactions of the Tf-Penetratin liposomes with the serum proteins and therefore, a greater release (non-significant) of the encapsulated drug as compared to the other Tf-CPP liposomes.

The cytotoxicity of the liposomes, at increasing phospholipid concentrations, was evaluated using MTT assay in Daoy, U87, and bEnd.3 cells. The rationale for selecting these tumor cell lines was based on the incidence and severity of these tumors in the human population which directly relates to the need for establishing a successful treatment strategy for these tumors. Glioblastoma multiforme is the highest grade of astrocytic tumors and is associated with very low survival rates (44). Also, medulloblastoma is a rapidly growing high grade tumor and is the most common type of embryonal tumors (45). The dual-functionalized liposomes were biocompatible, however, the liposomes considerably increased the cytotoxic potential of the anticancer drug, doxorubicin. In our previous study, we showed efficient biocompatibility of the Tf-PR-liposomes in bEnd.3 and glial cells up to 100nM phospholipid concentration (12). In this study, we used short chain CPPs and demonstrated an improved cellular biocompatibility up to 200nM phospholipid concentration. The Tf-TAT and Tf-Penetratin liposomes showed higher cell viability as compared to the Tf-Mastoparan liposomes. The cell viabilities of the dual-functionalized liposomes without doxorubicin were approximately 85–98%, however, incorporation of the drug reduced the viability of tumor cells to approximately 30–40% indicating efficient translocation of the anticancer drug into the tumor cells. The greater cytotoxic effect of Tf-Mastoparan liposomes could be partially attributed to the membrane disruptive potential of Mastoparan via binding to intracellular targets (46). The single ligand CPP-liposomes (without doxorubicin, Fig. S2) were observed be more cytotoxic as compared to the dual modified Tf-CPP liposomes (without doxorubicin, Fig S1). The greater cytotoxicity of the CPP-liposomes was due to the higher cationic charge of the CPP modified liposomes as compared to the dual-functionalized (Tf-CPP) or plain liposomes. In contrast, the negative charge of transferrin protein resulted in greater cell viabilities of Tf-liposomes as compared to the Tf-CPP liposomes.

Furthermore, the dual functionalized liposomes were transported across the cell membranes more efficiently as compared to the single ligand, Tf or CPP-liposomes. The cell uptake of Tf-CPP liposomes in this study (approximately 77–89% in bEnd.3 cells and approximately 90–98% in tumor cells after 1 h) was slower in comparison to the previously reported Tf-PR-liposomes (approximately 95% in bEnd.3 cells after 30 min) (12). This was ascribed to the presence of greater number of basic arginine residues in long chain poly-L-arginine as compared to the short chain CPPs used in this study. However, as mentioned above, the lower cationic charge of the CPPs used in this study considerably improved the biocompatibility of the liposomes. Binding and internalization of CPP-liposomes were driven by the cationic charge of CPPs and interaction of CPP-liposomes with heparan sulfate proteoglycans (12). In comparison, the translocation of dual-modified Tf-CPP liposomes was facilitated via specific receptor targeting and improved penetration effect of CPPs. Since doxorubicin, acts by nuclear localization, the uptake of doxorubicin encapsulating liposomes resulted in an intense overlap in the fluorescence regions of the drug and nuclei. Furthermore, the rate of liposomal uptake was dependent on the type of cells. A more rapid and greater uptake was observed in the tumor cell lines, Daoy and U87, while the bEnd.3 cells showed less and slower uptake. In entirety, the results emphasized the significance of dual-mechanism of uptake over receptor targeting or cell penetration alone (Fig. 2). The analysis of the uptake pathways performed using various inhibitors indicated that the transferrin conjugated (Tf and Tf-CPP) liposomes were primarily transported into the cells via clathrin mediated endocytosis, irrespective of the type of cells, while the uptake of CPP-liposomes was controlled by both macropinocytosis and clathrin coated vesicles (Fig. S8).

In this study, we followed an innovative approach in designing a simple and robust *in vitro* brain tumor model. The model was constructed by culturing the glioblastoma cells in the porous chitosan-PLGA scaffold and combining it with the tightly packed endothelial cell layer to simulate the *in vivo* tumor environment. The porous structure of the scaffold supported the growth of tumor cells in 3-dimensional milieu (47). Reportedly, the cells attach to the intertwined scaffold fibers and fill the spaces/pores within the scaffold to form a 3D tumor (48,49). The tightness of the tumor associated endothelial barrier was compared with the intactness of the endothelial barrier without the tumor scaffold and with glial cells on the abluminal side of the membrane. The lower transport of sodium fluorescein across the tumor associated endothelium *versus* the endothelial cells alone was partially ascribed to the physical contact of endothelial cells with scaffold in the *in vitro* brain tumor model *versus* the presence of only endothelial cells on the luminal surface of culture inserts (bEnd.3 model). Also, since the transport was based on the lysis of cells and release of fluorescent molecule, incomplete lysis of the tumor could also contribute to lower fluorescence intensity. However, significant reduction ($p < 0.05$)

in the transport of Na-F was observed across the *in vitro* BBB model, where primary glial cells were grown on the abluminal surface of the membrane with the endothelial cells inside the culture inserts (12). This was similar to the *in vivo* condition where the occurrence of tumor is associated with the increased permeability of the BBB (50). The paracellular transport of Na-F increased (non-significantly) after the transport of liposomes which could be due to the increased permeability of the barrier after interaction with the cationic peptide conjugated liposomes. However, the tightness of the endothelial barrier (decreased permeability of Na-F) was restored after incubation of the endothelial cell culture inserts with the 3D tumor in the presence of 20–30% serum. The TEER across the endothelial cell layer of the BBB model with bEnd.3 cells and glial cells was considerably higher as compared to the TEER across the endothelial cell layer of the tumor model and across the endothelial cell layer cultured alone. This was ascribed to the down regulation of tight junction proteins like occludin and claudin in the tumor associated endothelial barrier (51). Also, the absence of any glial cells, in the model with the endothelial cell culture alone, contributed to the formation of more leaky barrier due to the lack of the induction and maintenance of barrier properties (12,52). The dual-functionalized liposomes showed higher transport across the barrier layer with Tf-Penetratin liposomes demonstrating the maximum permeability. The cationic charge of penetratin and the presence of amphiphilic amino acids contributed to increased interaction of Tf-Penetratin liposomes with the endothelial membrane as compared to the Tf-TAT liposomes. The presence of transferrin triggered receptor mediated transcytosis across the endothelial membrane. In contrast, the lower cationic charge of the mastoparan peptide reduced the endothelial transcytosis of Tf-Mastoparan liposomes (non-significantly) as compared to the Tf-Penetratin liposomes. In addition, the transport of CPP and plain liposomes was lower in comparison to the Tf-CPP liposomes which could be attributed to the absence of dual-mechanism of cell uptake and greater entrapment of these liposomes in the endothelial cell layer.

The cationic polymers, macromolecules and cell penetrating peptides are considered to induce non-specific interactions with the erythrocytes after systemic administration that can affect the membrane integrity of erythrocytes and cause hemolysis (9,53). We evaluated the interaction of Tf-CPP liposomes with the erythrocytes by performing hemolysis assay. Both Tf-TAT and Tf-penetratin were observed to be non-toxic up to concentrations as high as 800 nmoles of phospholipids. However, Tf-Mastoparan liposomes demonstrated significantly higher ($p < 0.05$) hemolytic activity as compared to other Tf-CPP liposomes. This could be due to the cytolytic nature of the Mastoparan peptide (54). In addition, we anticipate that the presence of more hydrophobic amino acids in Mastoparan might increase the interaction of this peptide with the lipophilic erythrocyte membrane. Furthermore, the evaluation of *in vivo* biodistribution showed more rapid uptake of doxorubicin encapsulating Tf-Mastoparan liposomes in liver and spleen as compared to the Tf and the other Tf-CPP liposomes. The greater hydrophobicity of the mastoparan peptide and its potential to trigger non-specific interactions was considered to affect its uptake by the major macrophage organs. Also, the decrease in the concentration of the drug transported to the macrophage organs via Tf-Mastoparan liposomes was greater as compared to that transported via Tf-Penetratin and Tf-TAT liposomes, thus, indicating a more rapid clearance of Tf-Mastoparan liposomes from the system. Tf-Penetratin liposomes showed maximum transport of doxorubicin into brain (approximately 4% ID/g) *in vivo* followed by Tf-TAT liposomes (approximately 2.9% ID/g). The lower transport using Tf-Mastoparan liposomes, into brain, was attributed to the greater uptake of these liposomes by liver, spleen and lungs and therefore, lesser availability for transport to brain. The drug encapsulated in the negatively charged Tf-liposomes remained in circulation for long however, the penetration of drug into brain using Tf-liposomes was lesser as compared to the Tf-CPP liposomes. Apparently, the combination of Tf and CPP in dual-modified liposomes increased their penetration into brain. Plain liposomes were transported largely to liver and spleen and showed negligible transport of drug across BBB. The occurrence of Tf receptors in the major macrophage organs (liver, spleen and kidneys) can result in non-specific uptake of the transferrin conjugated liposomes by these organs (55,56). Also, a major portion of the intravenously administered delivery systems is eliminated via liver and spleen therefore, a large portion of these liposomes was transported to these organs. In addition, previous studies indicate increased interaction of cationic polymers and CPPs with the blood cells and their subsequent accumulation in lungs (9,38). The transport of drug encapsulated in the Tf-Mastoparan was more to the lungs than Tf-Penetratin or Tf-TAT liposomes. This was due to the greater interaction of these liposomes with the erythrocytes (Fig. 8). Since, the transport of drug encapsulated into the non-targeted CPP-liposomes, across the *in vitro* brain tumor model, was lower as compared to the transferrin receptor targeted Tf and Tf-CPP liposomes, these liposomes were not considered for *in vivo* evaluation of biodistribution. Evaluation of biodistribution of the water soluble drug encapsulated in the Tf-CPP liposomes, provides an insight into the *in vivo* fate and brain transport of the encapsulated agent in these liposomes. The enhanced permeability of the tumor associated brain endothelial barrier is anticipated to further increase the translocation of the targeted Tf-CPP liposomes into brain, *in vivo*.

CONCLUSIONS

The study illustrated the influence of three different CPPs on the cell uptake, tumor penetration and cytotoxic potential of Tf-receptor targeted liposomes. The results indicated that the incorporation of amphiphilic CPPs, TAT and Penetratin, on the surface of Tf-liposomes resulted in biocompatible formulations leading to efficient translocation of doxorubicin across cellular and brain endothelial barriers both *in vitro* and *in vivo*. The conjugation of hydrophobic CPP, Mastoparan, also resulted in improved cellular uptake of Tf-liposomes, however, the higher cytotoxicity and hemolytic activity of this peptide provided a strong evidence for restricting its use *in vivo*. The Tf-Penetratin liposomes showed maximum cell uptake and transport of the encapsulated drug, across the *in vitro* endothelial barrier, followed by the transport of Tf-Mastoparan liposomes. However, increased hemolytic activity of Tf-Mastoparan liposomes resulted in greater clearance of these liposomes by the macrophage system and therefore, less availability for penetration into the brain, *in vivo*. This research work is anticipated to provide significant contribution in the continuum of research that illustrates the influence of grafting the cell penetrating peptide to targeted liposomal delivery vector and forming near neutral vesicles for improving the delivery of therapeutics across the BBB. We anticipate that this study will contribute towards the development of high efficiency and low toxicity delivery systems and subsequently help to find new treatment strategies for CNS diseases (e.g., tumors, Alzheimer's disease and certain neuropsychiatric disorders).

ACKNOWLEDGMENTS AND DISCLOSURES

This work was supported by Fraternal Order of Eagles grant. We thank Dr. Erxi Wu, Department of Pharmaceutical Sciences, North Dakota State University, for providing tumor cell lines (Daoy and U87).

REFERENCES

1. Koren E, Torchilin VP. Cell-penetrating peptides: breaking through to the other side. Trends Mol Med. 2012;18:385–93.
2. Gupta B, Levchenko TS, Torchilin VP. Intracellular delivery of large molecules and small particles by cell-penetrating proteins and peptides. Adv Drug Deliv Rev. 2005;57:637–51.
3. Rooy IV, Mastrobattista E, Storm G, Hennink WE, Schiffelers RM. Comparison of five different targeting ligands to enhance accumulation of liposomes into the brain. J Control Release. 2011;150:30–6.
4. Emerich DF, Snodgrass P, Pink M, Bloom F, Bartus RT. Central analgesic actions of loperamide following transient permeation of the blood–brain barrier with Cereport (RMP-7). Brain Res. 1998;801: 259–66.
5. Scherrmann JM. Drug delivery to brain via the blood–brain barrier. Vasc Pharmacol. 2002;38:349–54.
6. Huwyler J, Wu D, Pardridge WM. Brain drug delivery of small molecules using immunoliposomes. Proc Natl Acad Sci U S A. 1996;93:14164–9.
7. Pardridge WM, Eisenberg J, Yang J. Human blood–brain barrier insulin receptor. J Neurochem. 1985;44:1771–8.
8. Oba M, Fukushima S, Kanayama N, Aoyagi K, Nishiyama N, Koyama H, *et al*. Cyclic RGD peptide-conjugated polyplex micelles as a targetable gene delivery system directed to cells possessing alphavbeta3 and alphavbeta5 integrins. Bioconjug Chem. 2007;18: 1415–23.
9. Sharma G, Modgil A, Layek B, Arora K, Sun C, Law B, *et al*. Cell penetrating peptide tethered bi-ligand liposomes for delivery to brain in vivo: biodistribution and transfection. J Control Release. 2013;167:1–10.
10. Zhong MQ, Hongyan L, Hongzhe U, Kwokping H. Targeted drug delivery via the transferrin receptor-mediated endocytosis pathway. Pharmacol Rev. 2002;54:561–87.
11. Cheng Y, Zak O, Alsen P, Harrison SC, Watz T. Structure of the human transferrin receptor-transferrin complex. Cell. 2004;116: 565–76.
12. Sharma G, Modgil A, Sun C, Singh J. Grafting of cell-penetrating peptide to receptor-targeted liposomes improves their transfection efficiency and transport across blood–brain barrier model. J Pharm Sci. 2012;101:2468–78.
13. Kibria G, Hatakeyama H, Ohga N, Hida K, Harashima H. Dual ligand modification of PEGylated liposomes shows better cell selectivity and efficient gene delivery. J Control Release. 2011;153: 141–8.
14. Varga CM, Wickham TJ, Lauffenburger DA. Receptor mediated targeting of gene delivery vectors: insights from molecular mechanisms for improved vehicle design. Biotechnol Bioeng. 2000;70:593–605.
15. Bolhassani A. Potential efficacy of cell-penetrating peptides for nucleic acid and drug delivery in cancer. Biochim Biophys Acta. 1816;2011:232–46.
16. Mae M, Myrberg H, EI-Andaloussi S, Langel U. Design of a tumor homing cell penetrating peptide for drug delivery. Int J Pept Res Ther. 2009;15:11–5.
17. Ziegler A, Nervi P, Durrenberger M, Seelig J. The cationic cell-penetrating peptide CPP TAT derived from the HIV-1 protein Tat is rapidly transported into living fibroblasts: optical, biophysical and metabolic evidence. Biochemistry. 2005;44:138–48.
18. Meng W, Kallinteri P, Walker DA, Parker TL, Garnett MC. Evaluation of poly (Glycerol-Adipate) nanoparticle uptake in an in vitro 3-D brain tumor co-culture model. Exp Biol Med. 2007;232:1100–8.
19. Murray S, Rooprai H, Selway R, Pilkington G. A novel three-dimensional "all human" in vitro brain tumor invasion model. Neuro-Oncology. 2005;7:307–8.
20. Deeken JF, Loscher W. The blood–brain barrier and cancer: transporters, treatment, and Trojan horses. Clin Cancer Res. 2007;13(6):1663–74.
21. Lewin M, Carlesso N, Tung CH, Tang XW, Cory D, Scadden DT, *et al*. Tat peptide-derivatized magnetic nanoparticles allow in vivo tracking and recovery of progenitor cells. Nat Biotechnol. 2000;18: 410–4.
22. Derossi D, Chassaing G, Prochiantz A. Trojan peptides: the penetratin system for intracellular delivery. Trends Cell Biol. 1998;8:84–7.
23. Pooga M, But C, Kihlmark M, Hallbrink M, Fernaeus S, Raid R, *et al*. Cellular translocation of proteins by transportan. J FASEB. 2001;15:1451–3.
24. Rousselle C, Smirnova M, Clair P, Lefauconnier JM, Chavanieu A, Calas B, *et al*. Enhanced delivery of doxorubicin into the brain via a

peptide- vector-mediated strategy: saturation kinetics and specificity. JPET. 2001;296:124–31.
25. Rea JC, Barron AE, Shea LD. Peptide-mediated lipofection is governed by lipoplex physical properties and the density of surface-displayed amines. J Pharm Sci. 2008;97:4794–806.
26. Miedel MC, Hulmes JD, Pan YEC. The use of fluorescamine as a detection reagent in protein microcharacterization. J Biochem Biophys Methods. 1989;18:37–52.
27. Yub E, Kojima C, Sakaguchi N, Harada A, Koiwai K, Kono K. Gene delivery to dendritic cells mediated by complexes of lipoplexes and pH-sensitive fusogenic polymer-modified liposomes. J Control Release. 2008;130:77–83.
28. Yamano S, Dai J, Yuvienco C, Khapli S, Moursi AM, Montclare JK. Modified Tat peptide with cationic lipids enhances gene transfection efficiency via temperature-dependent and caveolae-mediated endocytosis. J Control Release. 2011;152:278–85.
29. Rejman J, Bragonzi A, Conese M. Role of clathrin- and caveolae-mediated endocytosis in gene transfer mediated by lipo- and polyplexes. Mol Ther. 2005;12:468–74.
30. Vercauteren D, Vandenbroucke RE, Jones AT, Rejman J, Demeester J, De Smedt SC, *et al*. The use of inhibitors to study endocytic pathways of gene carriers: optimization and pitfalls. Mol Ther. 2010;18:561–9.
31. Nam HY, Kwon SM, Chung H, Lee SY, Kwon SH, Jeon H, *et al*. Cellular uptake mechanism and intracellular fate of hydrophobically modified glycol chitosan nanoparticles. J Control Release. 2009;135: 259–67.
32. Gaillard PJ, Voorwinden HV, Nielsen JL, Ivanov A, Atsumi R, Engman H, *et al*. Establishment and functional characterization of an in vitro model of the blood–brain barrier comprising a co-culture of brain capillary endothelial cells and astrocytes. Eur J Pharm Sci. 2001;12:215–22.
33. Fenke H, Galla HJ, Beuckmann CT. Primary cultures of brain microvessel endothelial cells: a valid and flexible model to study drug transport through the blood–brain barrier in vitro. Brain Res Brain Res Protoc. 2000;5:248–56.
34. Erben M, Decker S, Franke H, Galla HJ. Electrical resistance measurements on cerebral capillary endothelial cells—a new technique to study small surface areas. J Biochem Biophys Methods. 1995;30:227–38.
35. Fischer D, Li Y, Ahlemeyer B, Krieglstein J, Kissel T. In-vitro cytotoxicity testing of polycations: influence of polymer structure on cell viability and hemolysis. Biomaterials. 2003;24:1121–31.
36. Lee D, Powers K, Baney R. Physicochemical properties and blood compatibility of acylated chitosan nanoparticles. Carbohydr Polym. 2004;58:371–7.
37. Rodal SK, Skretting G, Garred O, Vilhardt F, Deurs BV, Sandvig K. Extraction of cholesterol with Methyl-b-Cyclodextrin perturbs formation of clathrin-coated endocytic vesicles. Mol Biol Cell. 1999;10:961–74.
38. Audouy SAL, de Leiji LFMH, Hoekstra D, Molema G. In vivo characteristics of cationic liposomes as delivery vectors for gene therapy. Pharm Res. 2002;19:1599–605.
39. Jones SW, Christison R, Bundell K, Voyce CJ, Brockbank SMV, Newham P, *et al*. Characterization of cell-penetrating peptide-mediated peptide delivery. Br J Pharmacol. 2005;145:1093–102.
40. Iden DL, Allen TM. In vitro and in vivo comparison of immunoliposomes made by conventional coupling techniques with those made by a new post-insertion approach. Biochim Biophys Acta. 2001;1513:207–16.
41. Moreira JN, Ishida T, Gaspar R, Allen TM. Use of the post-insertion technique to insert peptide ligands into preformed stealth liposomes with retention of binding activity and cytotoxicity. Pharm Res. 2002;19:265–9.
42. Chen Y, Liu L. Modern methods for delivery of drugs across the blood–brain barrier. Adv Drug Deliv Rev. 2012;64:640–65.
43. Roney CC, Kulkarni P, Arora V, Antich P, Bonte F, Wu A, *et al*. Targeted nanoparticles for drug delivery through the blood–brain barrier for Alzheimer's disease. J Control Release. 2005;108:193–214.
44. Krex D, Klink B, Hartmann C, Deimling AV, Pietsch T, Simon M, *et al*. German Glioma Network, long-term survival with glioblastoma multiforme. Brain. 2007;130:2596–606.
45. McNeil DE, Cote TR, Clegg L, Rorke BL. Incidence and trends in pediatric malignancies medulloblastoma/primitive neuroectodermal tumor: a SEER update: surveillance epidemiology and end results. Med Pediatr Oncol. 2002;39:190–4.
46. Saar K, Lindgren M, Hansen M, Eiriksdottir E, Jiang Y, Rosenthal-Aizman K, *et al*. Cell-penetrating peptides: a comparative membrane toxicity study. Anal Biochem. 2005;345:55–65.
47. Kim JB. Three-dimensional tissue culture models in cancer biology. Semin Cancer Biol. 2005;15:365–77.
48. Sourla A, Doillon C, Koutsilieris M. Three-dimensional type I collagen gel system containing MG-63 osteoblasts-like cells as model for studying local bone reaction caused by metastatic cancer cells. Anticancer Res. 1996;16:2773–80.
49. Bell E. Strategy for the selection of scaffolds for tissue engineering. Tissue Eng. 1995;1:163–79.
50. Provenzale JM, Mukundan S, Dewhirst M. The role of blood–brain barrier permeability in brain tumor imaging and therapeutics. Am J Roentgenol. 2005;185:763–7.
51. Ishihara H, Kubota H, Lindberg RL, Leppert D, Gloor SM, Errede M, *et al*. Endothelial cell barrier impairment induced by glioblastomas and transforming growth factor beta2 involves matrix metalloproteinases and tight junction proteins. J Neuropathol Exp Neurol. 2008;67:435–48.
52. Janzer RC, Raff MC. Astrocytes induce blood–brain barrier properties in endothelial cells. Nature. 1987;325:253–7.
53. Antohi S, Brumfeld V. Polycation-cell surface interactions and plasma membrane compartments in mammals. Interference of oligocation with polycationic condensation. Z Naturforsch C. 1984;39:767–75.
54. Cardozo AK, Buchillier V, Mathieu M, Chen J, Ortis F, Ladrire L, *et al*. Cell-permeable peptides induce dose- and length-dependent cytotoxic effects. Biochim Biophys Acta Biomembr. 2007;1768: 2222–34.
55. Deaglio S, Capobianco A, Cali A, Bellora F, Alberti F, Righi L, *et al*. Structural, functional, and tissue distribution analysis of human transferrin receptor-2 by murine monoclonal antibodies and a polyclonal antiserum. Blood. 2002;100:3782–9.
56. Jefferies WA, Brandon MR, Hunt SV, Williams AF, Gatter KC, Mason DY. Transferrin receptor on endothelium of brain capillaries. Nature. 1984;312:162–3.